Journal of Structural Geology 31 (2009) 1511–1524

Contents lists available at ScienceDirect

Journal of Structural Geology

journal homepage: www.elsevier.com/locate/jsg

The effects of fault orientation and fluid infiltration on fault rock assemblages at seismogenic depths

Silvia Mittempergher [a,*], Giorgio Pennacchioni [a], Giulio Di Toro [a,b]

[a] Dipartimento di Geoscienze, Università di Padova, Via Giotto 1, 35137 Padua, Italy
[b] Istituto Nazionale di Geofisica e Vulcanologia, Via di Vigna Murata 605, 00143 Rome, Italy

ARTICLE INFO

Article history:
Received 25 March 2009
Received in revised form
31 August 2009
Accepted 4 September 2009
Available online 12 September 2009

Keywords:
Fault mechanics
Pseudotachylyte
Cataclasite
Fault rocks
Fluids
Veining
Earthquakes
Adamello

ABSTRACT

The factors controlling the development of different types of fault rock assemblages and, more specifically, the formation of friction melts are still not fully understood. In this study we compared two exhumed strike–slip faults in the Adamello batholith (Southern Alps): the Gole Larghe and the Passo Cercen fault zones, active at 9–11 km depth and temperatures of 250–300 °C. Each fault zone consists of hundreds of sub-parallel strands exploiting pre-existing joints. The Gole Larghe fault strikes N105 ± 5° and is dextral; the fault rocks are cataclasites and widespread, centimetre-thick pseudotachylytes. The Passo Cercen fault strikes on average N130° and is formed by multiple fault horizons: fault segments striking N105°–N130° are mainly dextral, whereas faults striking N135°–N140° are mainly sinistral. Microstructural, mineralogical and geochemical investigations show that the fault rocks are cataclasites associated with thick epidote + K-feldspar + quartz veins and rare, millimetre-thick pseudotachylytes. Field evidence suggests that in both fault zones, the direction of the maximum horizontal stress σ_1 was N135°. The Gole Larghe fault strikes at about 30° to σ_1 and is favourably oriented for reactivation. By contrast, the Passo Cercen fault strikes at low angles to σ_1 and is unfavourably oriented for reactivation, therefore requiring the development of high pore pressures, as suggested by the occurrence of extensive epidote veining and hydraulic breccias. It is proposed that frictional melting in the Passo Cercen fault zone was inhibited by the development of high pore pressures and low effective normal stresses.

1. Introduction

The study of exhumed faults in the field provides complementary information to seismological, geophysical and experimental data for understanding fault plane processes and mechanics during earthquakes (Sibson, 1977; Scholz, 1988; Imber et al., 2001; Abercrombie et al., 2006; Di Toro et al., 2009 for a review). However, few exhumed faults can be proved to have been seismic. At present, only tectonic pseudotachylytes (fault rocks formed by solidified friction-induced melts produced during seismic slip in silicate rocks: Sibson, 1975; Spray, 1995) are unambiguously recognized as the signature of ancient earthquakes in exhumed faults (e.g. Cowan, 1999). Nevertheless, pseudotachylyte occurrences are not as widespread as seismic activity in the Earth crust (Sibson and Toy, 2006; Kirkpatrick et al., 2009). If pseudotachylytes in exhumed seismogenic faults are uncommon, this could be related to the occurrence of thermal pressurization of pore fluids (or other coseismic fault weakening mechanisms such as flash heating, e.g. Rice, 2006) along the fault surfaces which may impede frictional melting (Sibson, 1973; Lachenbruch, 1980; Andrews, 2002; Rice, 2006; Bizzarri and Cocco, 2006).

In this field-based study, the influence of fault orientation and pore fluids on the development of pseudotachylytes is investigated by comparing faults that were active close to the base of the seismogenic crust within the Adamello batholith in the Southern Alps, Italy. In the northern Adamello batholith, pseudotachylyte-bearing faults have already been described in detail along the Gole Larghe fault zone (Di Toro and Pennacchioni, 2004, 2005; Pennacchioni et al., 2006). In the present contribution, the Gole Larghe fault zone is compared with the Passo Cercen fault zone, located few kilometres to the north, where pseudotachylytes are rare and there is evidence of widespread fluid infiltration. We conclude that, in the case of the Passo Cercen fault zone, fault orientation was favourable for fluid infiltration which, in turn: (1) allowed hydraulically induced failure under low normal effective stresses; and (2) impeded the production of abundant pseudotachylytes.

2. Geological setting

The Adamello batholith is located within the central Southern Alps (Italy) close to the intersection of two major segments of the

* Corresponding author. Tel.: +39 49 827 1912; fax: +39 49 827 1868.
E-mail address: silvia.mittempergher@unipd.it (S. Mittempergher).

0191-8141/$ – see front matter © 2009 Elsevier Ltd. All rights reserved.
doi:10.1016/j.jsg.2009.09.003

Periadriatic Line: the Tonale Line to the north, and the Southern Giudicarie Line to the east (Fig. 1a). The Periadriatic Line separates the south-verging thrusts and folds of the Southern Alps, not affected by Alpine metamorphism, from the north-verging stack of Alpine metamorphic units (e.g. Schmid et al., 1989). The Adamello batholith is the largest Tertiary magmatic body intruded adjacent to the Periadriatic lineament ("Periadratic plutonism", Salomon, 1897). It is a composite pluton consisting of four main intrusions of dominantly tonalitic–granodioritic composition (Bianchi et al., 1970) (Fig. 1a), whose ages progressively young from south-west (Re di Castello: 42–38 Ma) to north-east (Presanella: 32–30 Ma) (Del Moro et al., 1983; Hansmann and Oberli, 1991; Viola, 2000; Viola et al., 2001; Mayer et al., 2003; Stipp et al., 2004). Within each intrusion, the overlap between U–Pb zircon ages and different mineral ages suggests a rapid cooling to the zircon fission track closure temperature (250 ± 50 °C) after emplacement (Pennacchioni et al., 2006). Ambient temperature before emplacement of the Adamello batholith is estimated to be about 250 °C, based on muscovite and biotite Rb/Sr dating of the pre-Permian basement rocks hosting the Adamello pluton, which indicates no or little post-Triassic reheating above 300–350 °C (De Capitani et al., 1994; Martin et al., 1996), on zircon fission track studies, which indicate cooling below 250 ± 50 °C during the Late Cretaceous (Viola et al., 2001) and on the illite crystallinity of Permian sandstones outcropping close to the Adamello pluton, which underwent, at most,

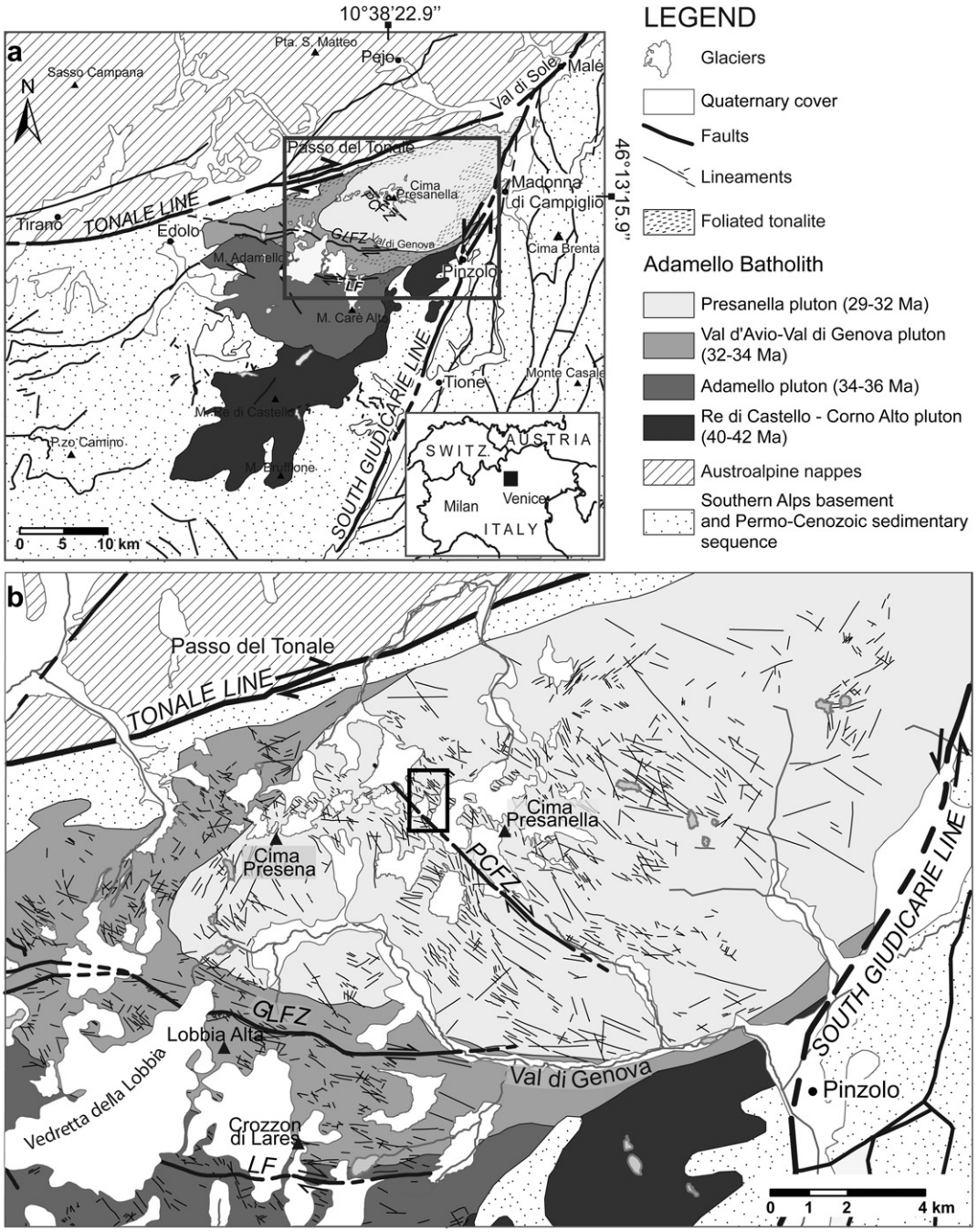

Fig. 1. Geological setting. (a) Simplified map of the central Alps and the Adamello batholith; GLFZ: Gole Large fault zone, PCFZ: Passo Cercen fault zone, LF: Lares fault. The rectangle is the area enlarged in Fig. 1b. (b) Schematic structural map, showing the main faults and the lineaments traced from aerial photographs. The wavy geometry of the GLFZ is due to the intersection with the irregular topography of the steeply (70°) dipping towards SSW fault plane. The rectangle is the area enlarged in Fig. 3a.

anchizonal metamorphic conditions (Riklin, 1985; see Pennacchioni et al., 2006 for discussion). Contact metamorphic mineral assemblages suggest pressures of >0.2 GPa in the northern aureole (Werling, 1992; Stipp et al., 2002), and as high as 0.35 GPa in the southern sector (John and Blundy, 1993).

2.1. Post-magmatic deformation of the Adamello pluton

Cooling of the Presanella and Avio plutons is believed to have been contemporary with dextral strike–slip motion along the Tonale Line (Stipp et al., 2004); the plutons show widespread solid state post-magmatic ductile and brittle deformation structures. A kilometer-thick belt of early post-magmatic foliated tonalites is developed along the north-eastern rim of the Presanella and Avio plutons and along the contact between the plutons in Val di Genova (Trener, 1906; Bianchi et al., 1970) (Fig. 1a). In the Avio pluton, the tonalite is cut by different sets of joints, intruded by aplitic dykes and decorated by biotite and An-rich plagioclase, suggesting temperatures of formation above or around 600 °C (Pennacchioni et al., 2006). Joints and aplitic dykes were first exploited by ductile amphibolite facies shear zones at $T > 500$ °C, as indicated by the stability of relatively An-rich plagioclase and biotite, the formation of strain-induced myrmekites and the crystallographic preferred orientation of the syn-kinematically recrystallized quartz aggregates (Pennacchioni, 2005). Joints were then exploited by pseudotachylyte- and cataclasite-bearing faults active at temperatures ranging between 250 and 300 °C, as indicated by the presence of chlorite and epidote assemblages (Di Toro and Pennacchioni, 2004). Lastly, zeolite-bearing faults ($T < 200$ °C) cut the previously described deformation structures (Pennacchioni et al., 2006).

The cataclasite–pseudotachylyte horizons are clustered defining some major fault zones, such as the Lares fault zone (LF), the Gole Larghe fault zone (GLFZ) and the Passo Cercen fault zone (PCFZ) (Fig. 1). The GLFZ is an E–W-trending, steeply dipping towards the SSW, dextral strike–slip fault extending from the Tonale Line into the Adamello pluton for about 20 km. In the Lobbia area (upper Val Genova), the GLFZ is about 500 m thick, with a total offset of 1 km distributed over a few hundred, sub-parallel main cataclastic horizons (Di Toro and Pennacchioni, 2005). The average fault dip is 60° towards N195° identical to the orientation of the main joint set outside the fault zone. The cataclasites are green and are enriched in epidote + K-feldspar + chlorite compared to the host tonalite. The same minerals fill millimetre-thick veins, which both pre-date and post-date cataclasites (Di Toro and Pennacchioni, 2004). Abundant pseudotachylytes occur as fault veins parallel to the cataclasite layers and injection veins intruding both the host tonalites and the cataclasites (Di Toro and Pennacchioni, 2004).

The pseudotachylytes of the GLFZ were dated using the stepwise heating ^{39}Ar–^{40}Ar method (Villa et al., 2000) on bulk pseudotachylytes, obtaining an average age of ca. 30 Ma (Pennacchioni et al., 2006). Fission track data on zircons indicate that exhumation of the Adamello batholith occurred after 22 Ma (Stipp et al., 2004; Viola, 2000). Therefore, seismic faulting occurred before substantial uplift of the pluton, at a depth of 9–11 km, estimated from the metamorphic assemblages preserved in the contact aureole and assuming an average rock density of 2650 kg m^{-3} (Di Toro et al., 2005).

3. The Passo Cercen fault zone

3.1. Structure of the fault zone

The PCFZ crops out on glacier-polished surfaces exposed NW of the Cima Presanella (3558 m) in the upper Val di Sole (Fig. 1a). The host rock is the Presanella tonalite (Bianchi et al., 1970), characterized by coarse (up to 2 cm long) prismatic hornblende set in a sub-centimetric matrix of plagioclase, quartz, biotite and K-feldspar. The tonalite is cut by pervasive joints with a main joint system (J1) consisting of two sets dipping either 66° to N040° (dominant set) or 56° to N218° (subordinate set) (stereoplot in Fig. 2a). Joints are spaced 0.1–15 m apart and are composed of segments 20–30 m long forming *en echelon* arrays (Fig. 2b). Joints are locally filled with quartz, epidote, K-feldspar and chlorite. A set of closely spaced joints (J2) striking NNE–SSW and steeply dipping towards ESE is discontinuously present within the area.

Cataclasite–pseudotachylyte-bearing faults, which are visible as lineaments striking from NW to WNW in aerial photographs (Fig. 3a), are clustered in the 1 km thick PCFZ. The faults have two main orientations, identical to those of the J1 joints: dipping 69° to N046° or 62° to N223°. The fault zone is formed by surfaces dipping preferentially towards SW, whereas joints outside the fault zone show the opposite, with a preponderance of joints dipping towards NE (Figs. 2a and 3b). In map view, NW-striking faults are formed of interconnected decametric segments, while WNW faults are more continuous (Fig. 3a). Lineations on NW and WNW fault planes plunge gently (about 30°) towards the SE or NW (Fig. 3c). The separation of offset markers such as mafic enclaves and magmatic bands along faults ranges from few centimetres up to 15 m and indicate both dextral and sinistral senses of offset; the switch in the sense of shear of the faults occurs around a strike of N135° (Fig. 3d); the overlapping of the dextral and sinistral faults suggests that the faults were oriented very close to the direction of σ_1.

Within the PCFZ, individual faults typically consist of a cataclasite layer ranging in thickness from millimetres to several

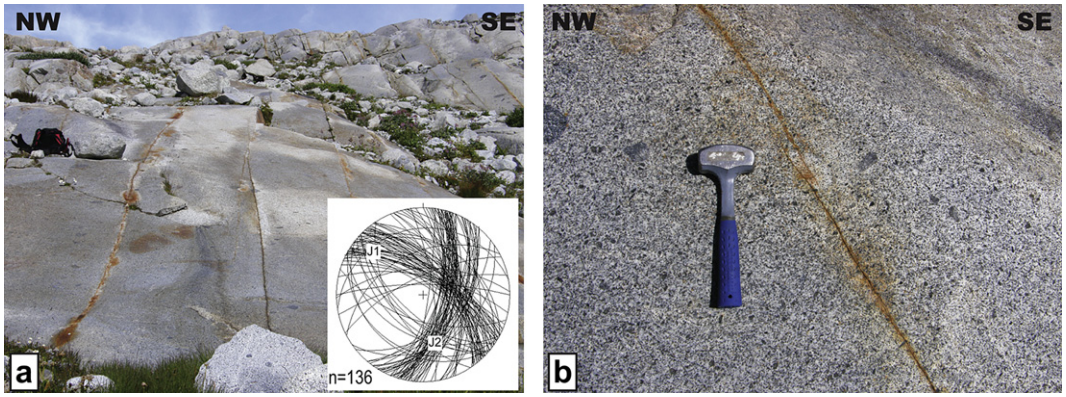

Fig. 2. Joints in the Passo Cercen fault zone area. (a) Joints of the main system (J1 in the inserted stereoplot) are formed by continuous and widely spaced segments; lower hemisphere, equal area projection stereoplot. (b) Details of the linkage between two parallel joint strands (J1) organized in an *en echelon* fashion.

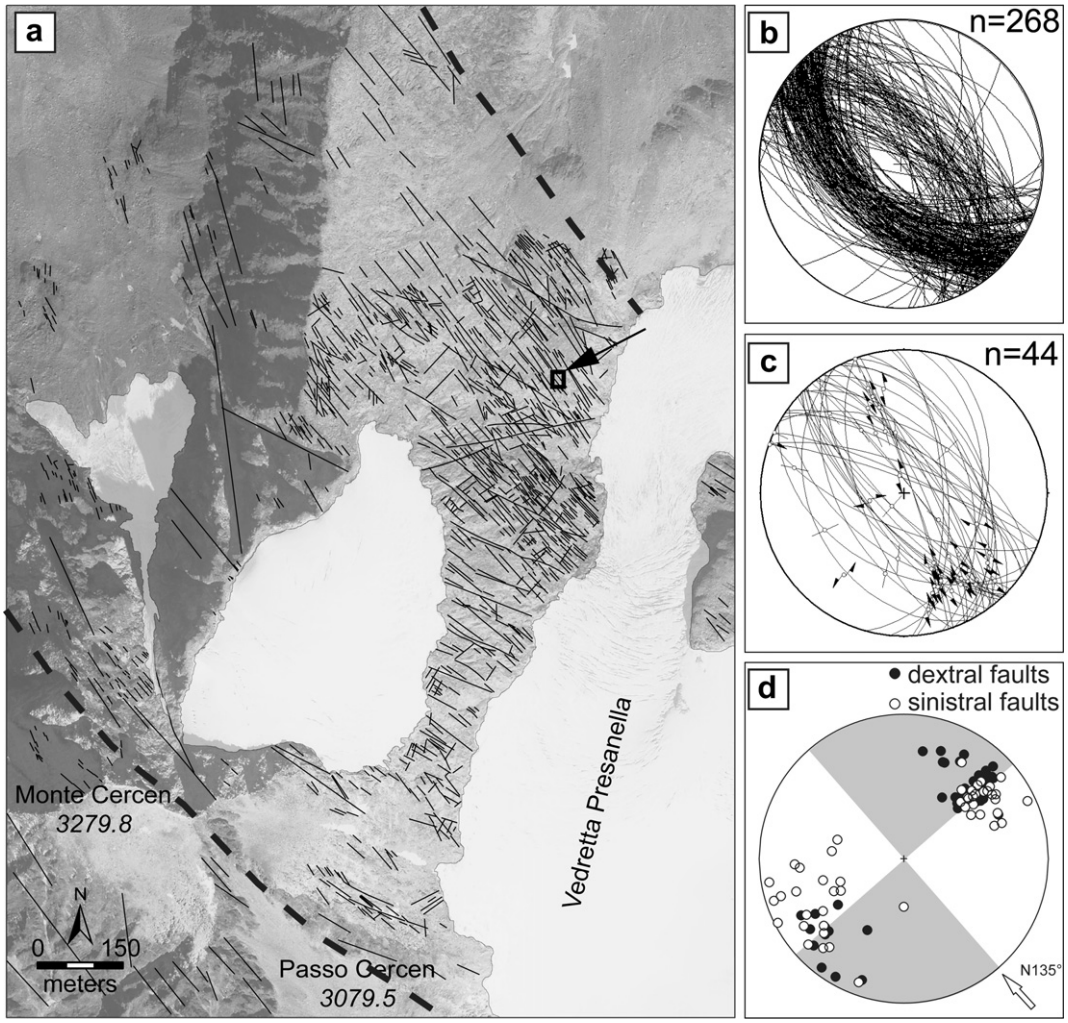

Fig. 3. Structural data from the PCFZ. (a) The internal architecture of the PCFZ, reconstructed from high resolution aerial photographs. Dashed lines are the limits of the fault zone. Some WNW-striking faults are outlined by narrow (2–3 m wide) troughs resulting from the intense fracturing and alteration of the fault rock assemblage, formed by the coalescence of multiple fault planes overprinted by late-stage zeolites. The small rectangle indicated by an arrow outlines the area of Fig. 5. (b) Stereoplot of cataclasite–pseudotachylyte-bearing faults (all data). (c) Stereoplot of cataclasite–pseudotachylyte-bearing faults (lineated faults); slickenlines are gently dipping towards SE or SW, with some dip slip planes. (d) Equal area, lower hemisphere cumulative plot of poles to fault planes separated by shear sense; the shaded and white quadrants represent the orientation ranges of faults with respectively sinistral and dextral shear sense. The overall switch in shear sense occurs around N135°.

decimetres. Faults are continuous for a few tens of meters and are spaced less than 1 m to 10–15 m apart (Fig. 4a). Many faults with a spacing of less than few meters are linked by a network of secondary shear and tensional fractures, whereas faults spaced several meters apart consist of sharp isolated structures (Fig. 4b).

A selected outcrop of the fault zone has been mapped at a scale of 1:10 (Fig. 5). In this outcrop, the sense of shear along the faults can be locally determined by the offset of basic enclaves and by the geometry of the secondary fracture network. Sinistral faults mostly strike NW whilst dextral faults strike WNW. In the southern part of the map, a dextral and sinistral fault set intersect each other at an angle of about 30° (Fig. 5a) and thin, discontinuous tensional fractures bisect the dihedral angle between the two faults. Along strike, faults show variations in thickness, due to the linkage between adjacent *en echelon* joint strands (Fig. 5b, see Fig. 2).

3.2. Field description of the fault rocks

The fault rocks are predominantly cataclasites, ranging in colour from dark (Fig. 6a) to light-yellowish green (Fig. 6b and c) and rare black pseudotachylytes (Fig. 6b).

Dark green cataclasites are thin (up to a few centimetres), continuous layers of ultracataclasite–cataclasite–protocataclasite (Fig. 6a). Boundaries with the host rock are either sharp, or transitional through a volume of fractured and altered tonalite.

Pseudotachylytes are distinguishable in the field from ultracataclasites on the basis of their black colour and presence of injection veins, even though only microstructural features are indicative of their melt origin. Pseudotachylytes occur as thin (up to 1 cm thick), discontinuous fault veins developed within cataclasite or at the cataclasite–tonalite boundary (Fig. 6b); injection veins are rare and up to a few centimetres long. Pseudotachylytes are mostly spatially associated with dark green cataclasites, but some very thin (<4 mm) pseudotachylyte fault veins have been found in association with light green cataclasites.

Light green cataclasites are more common in the southern part of the studied fault zone section showed in Fig. 3. They are up to 80 cm thick and are associated with pervasive alteration of the adjacent tonalite, as evidenced by its greenish colour (see Section 3.3.2) (Fig. 6c and d). Cataclasites are either homogeneous, fine grained ultracataclasites, or are formed by a breccia of angular tonalite clasts. In this sector, cataclasites are often associated with

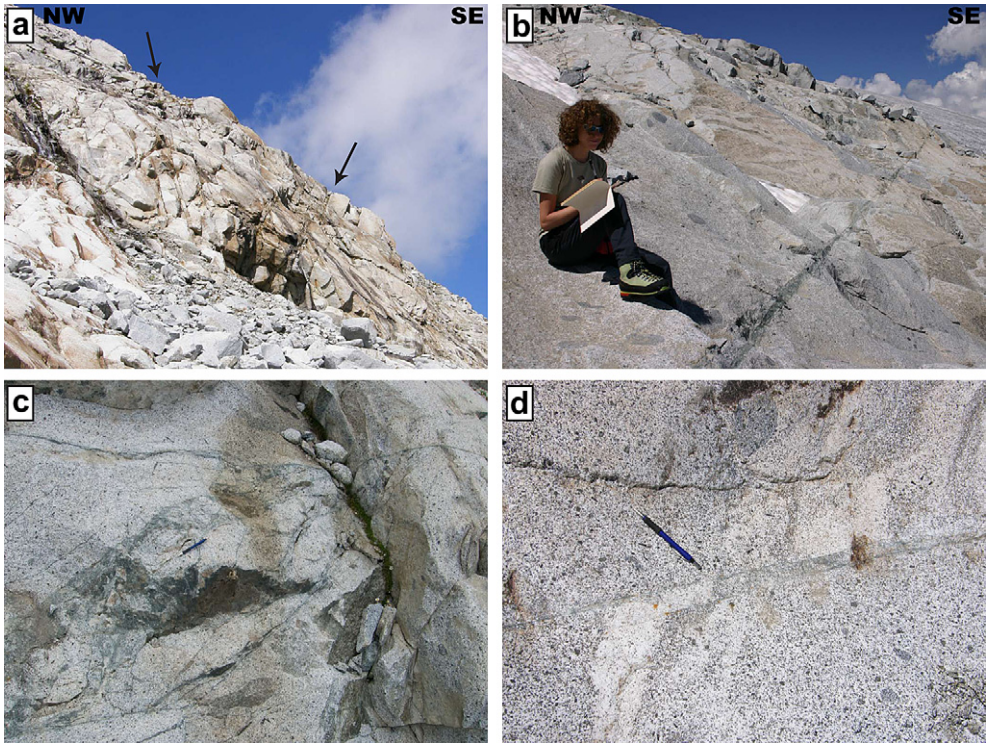

Fig. 4. Exposures of the PCFZ. (a) Faults exploit both joints dipping towards NE and SW (arrows). Note the variable spacing between adjacent fault zones. (b) Widely spaced faults are very sharp and continuous along strike. (c) Linkage between parallel fault strands, spaced about 1 m apart, occurs by intense fracturing of the "sandwiched" intervening panel of tonalite. (d) Dextral offset of a leucocratic magmatic band.

green, epidote-bearing veins branching at low angles from the fault planes (Fig. 6d).

3.3. Microstructure of the fault zone rocks

3.3.1. Damaged host tonalite

The Presanella tonalite consists of An_{52-59} plagioclase (45.8% in volume), quartz (23.4%), biotite (16%), hornblende (9.1%), K-feldspar (2.1%) and accessory apatite, allanite and titanite (Bianchi et al., 1970). Outside the damage zone, the texture is characterized by centimetre long, prismatic poikilitic hornblende, zoned euhedral plagioclase with Ca-rich nuclei and interstitial quartz and K-feldspar; the contacts between K-feldspars and quartz grains sometimes display myrmekite lobes. The tonalite close to cataclasites is altered and bleached for a few centimetres in thickness. In the altered tonalite: (1) plagioclase is partially replaced by an aggregate of epidote and fine white mica (saussuritization); (2) quartz is fractured and shows local patchy/undulose extinction, deformation lamellae (mostly related to fluid inclusion trails) and very incipient development of fine grained (20–50 μm) new grains; (3) magmatic biotite is kinked and broken down to chlorite and titanite (Fig. 7a), and (4) hornblende is fractured and substituted by actinolite, in particular along fractures and cleavage planes. The tonalite close to faults is commonly foliated due to the development of wavy pressure solution seams, sealed by chlorite, titanite and Ti–Fe oxides, branching at low angles to the fault planes and localized in Riedel fractures. The microstructures and the mineral assemblages described here suggest greenschist facies conditions, which are likely representative of those found close to the brittle–ductile transition.

3.3.2. Cataclastic rocks

Individual faults are associated with the development of protocataclasites, cataclasites and ultracataclasites. Protocataclasites are formed by large polymineralic fragments, slightly rotated and separated by thin cataclasite layers. Cataclasites are matrix-supported rocks, with angular clasts of quartz, plagioclase, K-feldspar and reworked precursor cataclasite (Fig. 7c). In some cases, the cataclasites have a wriggled foliation oriented at a low angle to the fault boundary. Ultracataclasites are thin (up to few millimetres) layers of highly comminuted material with a few rounded clasts. Under the Scanning Electron Microscope (SEM), the outlines of quartz clasts are commonly cuspate–lobate and corroded. The matrix is composed of chlorite, epidote, actinolite, Ti-poor biotite, K-feldspar and albite with textural evidence for static growth (e.g. presence of randomly oriented poikilitic epidote and acicular actinolite, Fig. 7d). In the matrix of some fault horizons, the growth of hydrothermal minerals (usually epidote, in grains of $<$100 micron in size) overprints the cataclasite texture. In such cases, we distinguished cataclasites from veins based on: (i) field evidence (e.g. cataclasite-bearing fractures offset structural markers, see above); and (ii) microstructural evidence (e.g. presence of relict cataclastic texture, such as comminuted grains).

3.3.3. Veins and implosion hydraulic breccias

The veins are filled with epidote, quartz, K-feldspar, albite and chlorite. Crystals in veins are blocky, suggesting that vein opening was faster than mineral growth (Passchier and Trouw, 2005). Quartz, albite and K-feldspar have mostly equidimensional habits, sometimes elongated; epidote crystals are acicular, and are either randomly oriented (Fig. 7e), or arranged perpendicular to the vein margins. Some veins have jigsaw puzzle textures formed by angular clasts of tonalite and cataclasite with little or no internal clast deformation and well-sorted clast size distributions (Fig. 7f). The fragmented clasts are suspended in an exotic hydrothermal cement of epidote, chlorite, K-feldspar, albite and quartz (Fig. 7f). The above microstructures are typical features of implosion hydraulic breccias

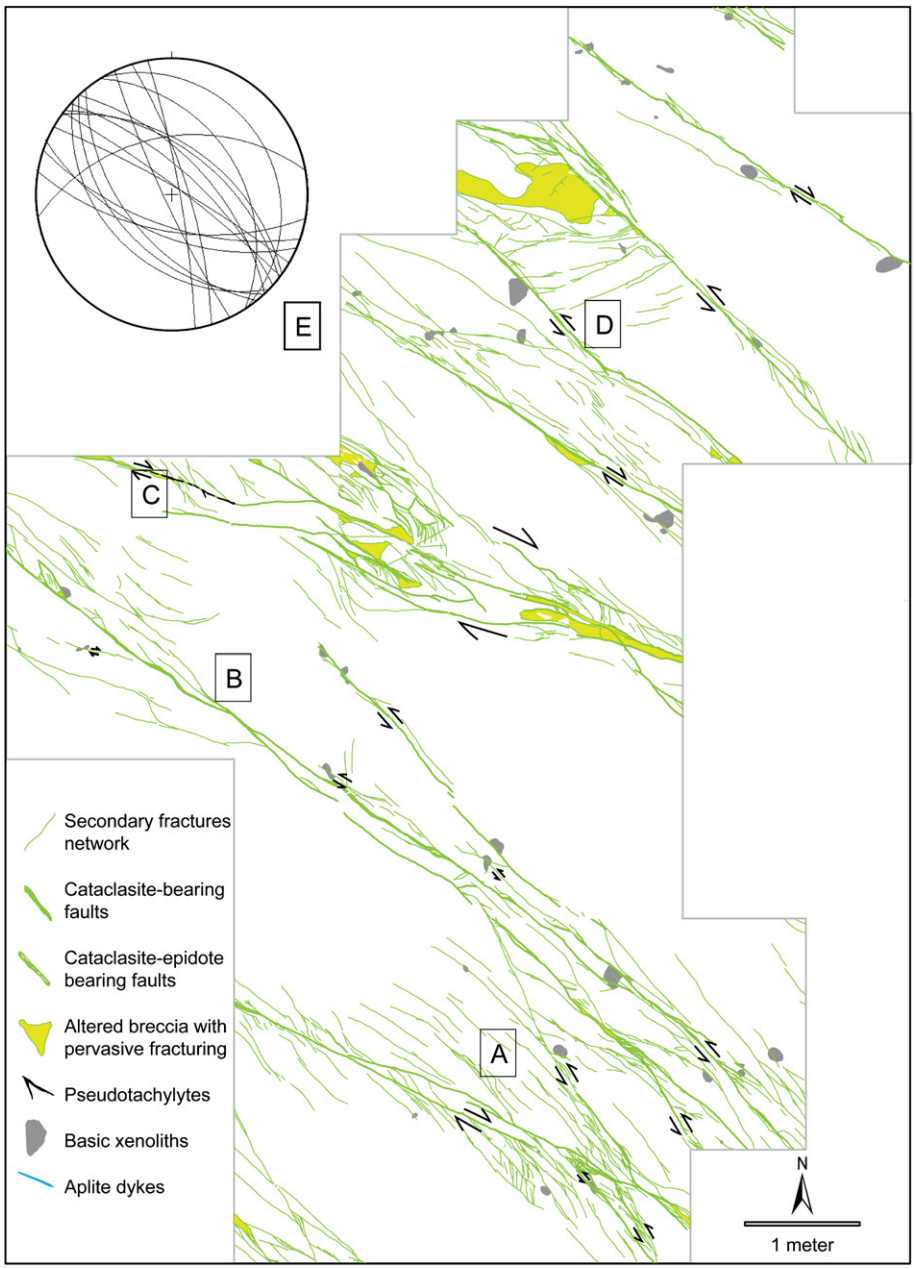

Fig. 5. High resolution surface map of the PCFZ (the map was drawn at 1:10 scale using a rigid frame of 1 m^2). (A) Intersection between two conjugate fault strands, with opposite sense of shear. (B) Variations in thickness along strike, due to linkage of adjacent *en echelon* segments. (C) Fault segment carrying pseudotachylyte, with a centimetre-long injection vein. (D) Faults spaced about 1 m apart linked by high angle fractures and domains of fragmented and altered tonalite. (E) Stereoplot of the fault planes represented in the surface map. Equal area, lower hemisphere plot.

according to the genetic classification of Sibson (1986) and could be classified as cement-supported chaotic breccias, following Woodcock and Mort (2008).

3.3.4. Pseudotachylytes

Pseudotachylytes of the PCFZ show microstructures typical of rapid cooling of a melt (e.g. Magloughlin and Spray, 1992; Di Toro and Pennacchioni, 2004; Di Toro et al., 2004), such as the development of flow structures, spherulites, plagioclase and biotite microlites, and a cryptocrystalline matrix (Fig. 7g and h). Clasts are rounded to angular and consist of quartz, plagioclase and K-feldspar. Under the Field Emission SEM the cryptocrystalline matrix is seen to comprise an aggregate of biotite, titanite and K-feldspar. Spherulitic aggregates form around quartz, plagioclase and K-feldspar clasts, as rims of radially arranged aggregates of plagioclase microlites and quartz. Spherical amygdale-like features filled by quartz and K-feldspar are often found dispersed in the pseudotachylyte matrix (Fig. 7h).

3.4. Geochemistry and mineralogy

X-ray fluorescence (XRF) and X-ray powder diffraction (XRPD) analyses were conducted on the cataclasites and host tonalite. Elemental XRF analyses show that light green cataclasites are highly enriched in Fe^{3+}, Ca, K and LILE (Rb, Sr, Ba) compared to the host rock (Table 1). Dark green cataclasites have less scattered elemental compositions and are enriched in Na with respect to unaltered tonalite. The relative change in major element

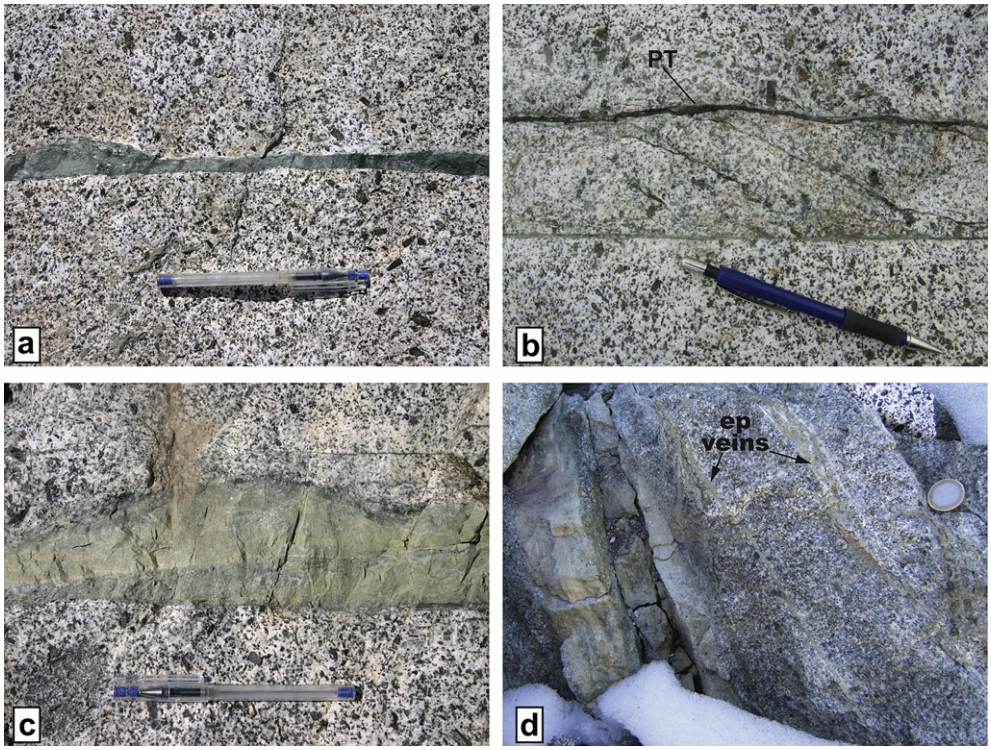

Fig. 6. Fault rocks from the PCFZ. (a) Dark green cataclasite; the edges with the host tonalite are sharp. (b) Paired faults, linked by oblique fractures, decorated by pseudotachylyte (PT) and dark green cataclasite. The secondary Riedel shear type fractures are decorated by cataclasite. The tonalite adjacent to the faults is bleached. (c) Thick light green cataclasite, composed of multiple layers. (d) Light green cataclasite, associated with epidote veins, oriented at low angle to the cataclasite. The tonalite adjacent to the fault and veins is strongly altered and has greenish colour. (For interpretation of references to colour in this figure legend the reader is referred to web version of the article).

composition is reflected in the abundances of minerals cementing the cataclasite matrix, determined from XRPD analysis (Fig. 8).

4. Passo Cercen fault zone vs. Gole Larghe fault zone

The scarcity of pseudotachylytes in the PCFZ and their abundance in the GLFZ (Fig. 9a and b) is a major difference between the fault zone rocks; the possible reasons for this difference in the two fault zones will be discussed in this section.

The GLFZ and PCFZ developed under similar ambient conditions at the base of the seismogenic crust during the final stages of cooling of the Avio and Presanella plutons and before their exhumation (Pennacchioni et al., 2006). The occurrence of sub-horizontal roof pendants in the inner parts of the Southern Adamello batholith (Brack, 1983), suggests that no tilting occurred during exhumation of the plutons from seismogenic depths. The depth of faulting is estimated at 9–11 km (Di Toro et al., 2005) and the ambient temperature was about 250 °C, as suggested by the presence of local incipient bulging recrystallization in quartz associated with cataclastic deformation, by the greenschist facies mineral assemblage (epidote, chlorite, K-feldspar, actinolite, albite) cementing the cataclasites (Fig. 9c and d) and the onset of stress induced solution-precipitation processes (i.e. presence of pressure solution seams) in both fault zones (Di Toro and Pennacchioni, 2005). The texture of the cataclasite matrix suggests precipitation under static conditions. The occurrence of reworked clasts of cemented cataclasite indicates that cementation was syn- to post-deformational. The host rock of both fault zones is tonalite (Table 1), though the Presanella tonalite (PCFZ) contains hornblende, which is absent in the Avio tonalite (GLFZ). Cataclasitic deformation was assisted by extensive percolation of fluids and pervasive precipitation of epidote + K-feldspar + chlorite ± actinolite and the occurrence of pressure-solution related microstructures in both faults (Fig. 9c and d). The extensive fluid-assisted alteration of cataclasites is attested by their enrichment in LILE and loss of Na and Fe^{3+} (Di Toro and Pennacchioni, 2005) compared to the host tonalites in both fault zones. The isocon diagrams (Grant, 2005) of Fig. 9e and f highlight the changes in major and trace elements of the fault rocks relative to the host tonalite due to interaction with fluids. The comparison between the cataclasite compositions of the PCFZ and GLFZ shows a larger data scattering in the former case, which is consistent with a stronger fluid-induced alteration in the fault rocks of the PCFZ compared to those of the GLFZ. This interpretation is based on the evidence that fluid flow was localized along fault horizons and that the fluid transfer between host and fault rocks could not equilibrate the compositional differences, as has been seen in other fault zones (e.g. Jefferies et al., 2006).

Both faults exploited pre-existing joints (Di Toro and Pennacchioni, 2005); the GLFZ exploits joints striking on average N105° whereas the PCFZ exploits joints striking on average N130°. The plane bisecting the average orientation of dextral and sinistral fault segments in the PCFZ strikes approximately at N135°. Since these are all strike slip faults, this orientation should correspond to the direction of the maximum horizontal stress σ_1 during faulting. A similar orientation of the regional σ_1 is inferred for the GLFZ (Di Toro and Pennacchioni, 2005). An identical shortening direction could also be inferred from the orientation of the flattening zones (Pennacchioni and Mancktelow, 2007) formed at the intersection between conjugate ductile shear zones exploiting the different sets of joints during the high temperature stages of pluton cooling preceding the cataclastic faulting (Pennacchioni, 2005) (Fig. 10). The orientation of σ_1 about N135° corresponds to the main regional compressive stress active in this area during the collisional stage of the Alpine orogeny (Castellarin et al., 2006; Castellarin and Cantelli, 2000). The different orientation of the fault

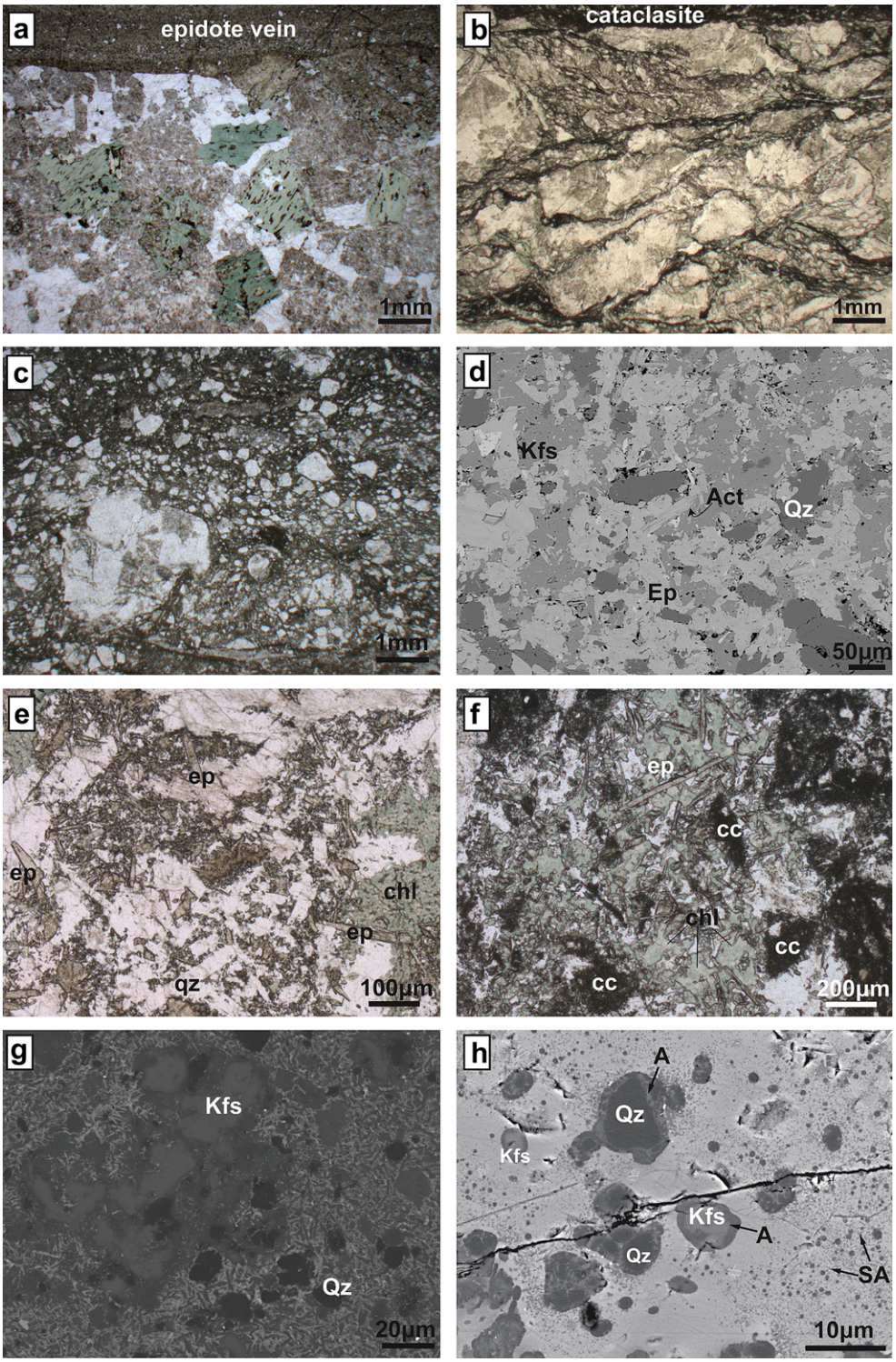

Fig. 7. Microstructures in the Passo Cercen fault rocks. (a) Altered tonalite adjacent to an epidote-bearing vein. Biotite is broken down to chlorite (green) and titanite aggregates, plagioclase is saussuritized (optical microscope, plane polarized light). (b) Close to cataclasites, tonalite is fractured and foliated due to the formation of wriggled surfaces cemented by chlorite, titanite, actinolite and remnants of biotite (optical microscope, plane polarized light). (c) Cataclasite is formed by angular clasts in a microcrystalline matrix (optical microscope, plane polarized light). (d) Cataclasite matrix, characterized by grain size on the order of the tens of micron and evidence of static growth and interactions with percolating fluids: quartz clasts have lobate edges, epidote has poikilitic texture, actinolite is acicular and is randomly oriented (Back Scatter Electron-SEM image). (e) Epidote (ep), chlorite (chl) and quartz (Qz)-bearing vein cutting altered tonalite; minerals sealing the vein are randomly oriented (optical microscope, plane polarized light). (f) The texture of a vein in cataclasite; randomly oriented, prismatic epidote crystals are floating in an aggregate of chlorite, plagioclase and quartz with blocky texture. Clasts of cataclasite (cc) are suspended in the vein (optical microscope, plane polarized light). (g) Microstructure of pseudotachylyte: partially melted K-feldspar clasts and rounded quartz clasts are immersed in a matrix composed by the fine intergrowth of biotite and plagioclase microlites (Back Scatter Electron-SEM image). (h) Detail of a pseudotachylyte characterized by a cryptocrystalline, bright matrix composed mainly of biotite, with dispersed small, spherical (amygdale-like) aggregates of plagioclase and silica (SA); quartz (Qz) and K-feldspar (Kfs) rounded clasts are rimmed by an aggregate of plagioclase and silica (A) (Field Emission Back Scatter Electron-SEM image). (For interpretation of references to colour in this figure legend the reader is referred to web version of the article).

Table 1
X-ray fluorescence analyses of fault and host rocks of the PCFZ and the GLFZ; PT, pseudotachylytes, CC, cataclasites. The data for the GLFZ are from Pennacchioni et al. (2006).

Rock type area	Avio tonalite		PT Avio		CC Avio		Presanella tonalite		Dark g. CC	Light g. CC	
	GLFZ		GLFZ		GLFZ		PCFZ		PCFZ	PCFZ	
	$n=5$	$n=5$	$n=5$	$n=5$	$n=4$	$n=4$	$n=3$	$n=3$	$n=1$	$n=3$	$n=3$
Wt%	Mean	*S.d.*	Mean	*S.d.*	Mean	*S.d.*	Mean	*S.d.*		Mean	*S.d.*
SiO_2	66.56	*0.84*	62.52	*1.54*	61.83	*2.51*	61.83	*0.23*	60.75	60.61	*10.10*
TiO_2	0.46	*0.04*	0.56	*0.05*	0.56	*0.14*	0.74	*0.02*	0.70	0.34	*0.16*
Al_2O_3	16.53	*0.33*	16.83	*0.24*	17.03	*0.84*	16.41	*0.02*	16.63	15.94	*3.58*
FeO	3.41	*0.26*	3.50	*0.41*	3.41	*0.38*	5.06	*0.14*	3.93	1.45	*1.04*
Fe_2O_3	0.33	*0.07*	1.10	*0.43*	1.18	*0.42*	0.40	*0.13*	0.67	4.05	*2.20*
MnO	0.10	*0.01*	0.12	*0.01*	0.13	*0.01*	0.11	*0.00*	0.17	0.10	*0.04*
MgO	1.57	*0.16*	1.89	*0.14*	1.88	*0.30*	2.35	*0.05*	2.64	0.82	*0.68*
CaO	4.44	*0.13*	3.85	*0.30*	3.86	*1.12*	5.67	*0.15*	6.13	8.77	*4.15*
Na_2O	2.95	*0.05*	2.47	*0.76*	1.69	*0.56*	2.62	*0.06*	6.36	0.85	*0.16*
K_2O	2.20	*0.10*	3.73	*1.27*	6.10	*1.37*	2.26	*0.16*	0.42	5.17	*1.14*
P_2O_5	0.11	*0.01*	0.13	*0.01*	0.13	*0.01*	0.13	*0.01*	0.10	0.07	*0.02*
L.O.I.	*0.91*	*0.06*	*2.77*	*0.71*	*2.02*	*0.52*	*1.47*	*0.11*	*0.95*	*1.44*	*0.43*
Tot	99.56	*0.12*	99.46	*0.16*	99.80	*0.35*	99.05	*0.03*	99.45	99.60	*0.15*
ppm											
Sc	14	*4*	16	*1*	17	*1*	14	*0*	10	7	*2*
V	58	*6*	71	*6*	77	*13*	106	*4*	99	166	*80*
Cr	13	*3*	27	*13*	24	*17*	14	*2*	12	27	*27*
Co	8	*1*	7	*3*	7	*2*	195	*15*	124	147	*62*
Ni	9	*3*	14	*8*	12	*9*	5	*0*	6	7	*6*
Cu	6	*2*	12	*11*	8	*5*	53	*20*	32	18	*23*
Zn	57	*5*	81	*28*	61	*11*	45	*0*	61	9	*11*
Ga	22	*2*	22	*4*	22	*5*	5	*0*	5	11	*7*
Rb	90	*11*	265	*149*	186	*23*	99	*1*	13	190	*32*
Sr	225	*9*	226	*16*	229	*25*	208	*6*	279	294	*128*
Y	26	*5*	30	*2*	39	*9*	25	*0*	22	19	*10*
Zr	117	*9*	135	*4*	126	*12*	137	*5*	137	65	*29*
Nb	10	*1*	12	*1*	12	*1*	11	*0*	11	6	*2*
Ba	375	*23*	447	*28*	740	*91*	343	*26*	285	573	*74*
La	30	*4*	39	*7*	38	*8*	29	*9*	29	16	*6*
Ce	53	*14*	66	*9*	68	*8*	43	*10*	37	35	*10*
Nd	23	*7*	22	*8*	24	*10*	15	*1*	20	10	*0*
Pb	29	*11*	37	*12*	32	*10*	5	*0*	5	7	*4*
Th	10	*2*	12	*1*	10	*2*	3	*0*	3	3	*0*
U	3	*0*	9	*5*	7	*1*	3	*0*	3	3	*1*

segments with respect to the maximum horizontal stress appears to be the most striking difference between the fault zones. The possible mechanical implications of this difference and influence on the development of the fault rock assemblages are discussed in the following section.

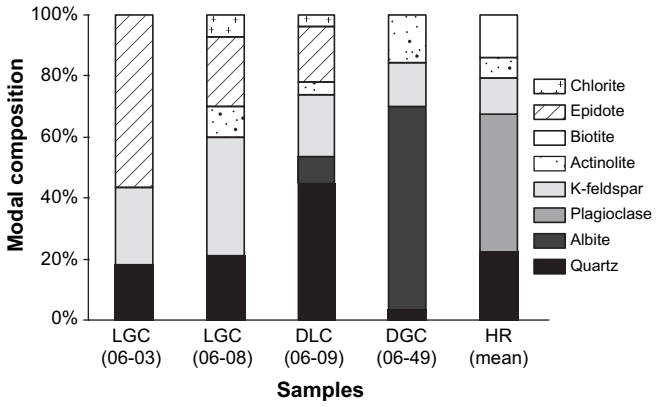

Fig. 8. Semi-quantitative modal composition of cataclasites and host tonalite from X-ray powder diffraction analyses (LGC: light green cataclasite, DLC: dark and light green cataclasite, DGC: dark green cataclasite, HR: host rock). The mineral composition of the cataclasites is strongly variable in the analysed samples. The reported modal compositions are based on the mathematical elaboration of the XRPD spectra. Since we did not use an internal standard, the analyses are semi-quantitative. (For interpretation of references to colour in this figure legend the reader is referred to web version of the article).

5. Discussion

The GLFZ and PCFZ were active in similar host rocks (tonalite), geochemical environment and P–T conditions, as discussed in the previous section. The faults have different orientations, which is determined by the attitude of pre-existing joints. We discuss below how fault orientation could affect the magnitude of the effective stresses normal to the fault surfaces and, as a consequence, the type of fault rock assemblages that may develop.

Tectonic pseudotachylytes form by the melting of fault and host rocks due to frictional heating along a fault surface during seismic slip (i.e. slip rates on average of about 1 m s^{-1}). The work done during faulting is (Kostrov and Das, 1988):

$$W_f = Q + U_s \quad (1)$$

where Q is heat and U_s is surface energy for gouge and fracture formation. Since U_s is considered negligible (Lockner and Okubo, 1983), the majority (>95%) of the work is converted to heat (Scholz, 2002). In the case of the Gole Larghe fault zone, this assumption was confirmed using a microstructural study of a pseudotachylyte-bearing fault (Pittarello et al., 2008). Thus, the amount of heat generated during seismic slip for unit area of the fault is (Price and Cosgrove, 1990):

$$W_f = \mu\left(\sigma_n - p_p\right)d \approx Q \quad (2)$$

Where μ is the friction coefficient, σ_n is the stress normal to the fault plane, p_p is the pore pressure and d is the coseismic slip.

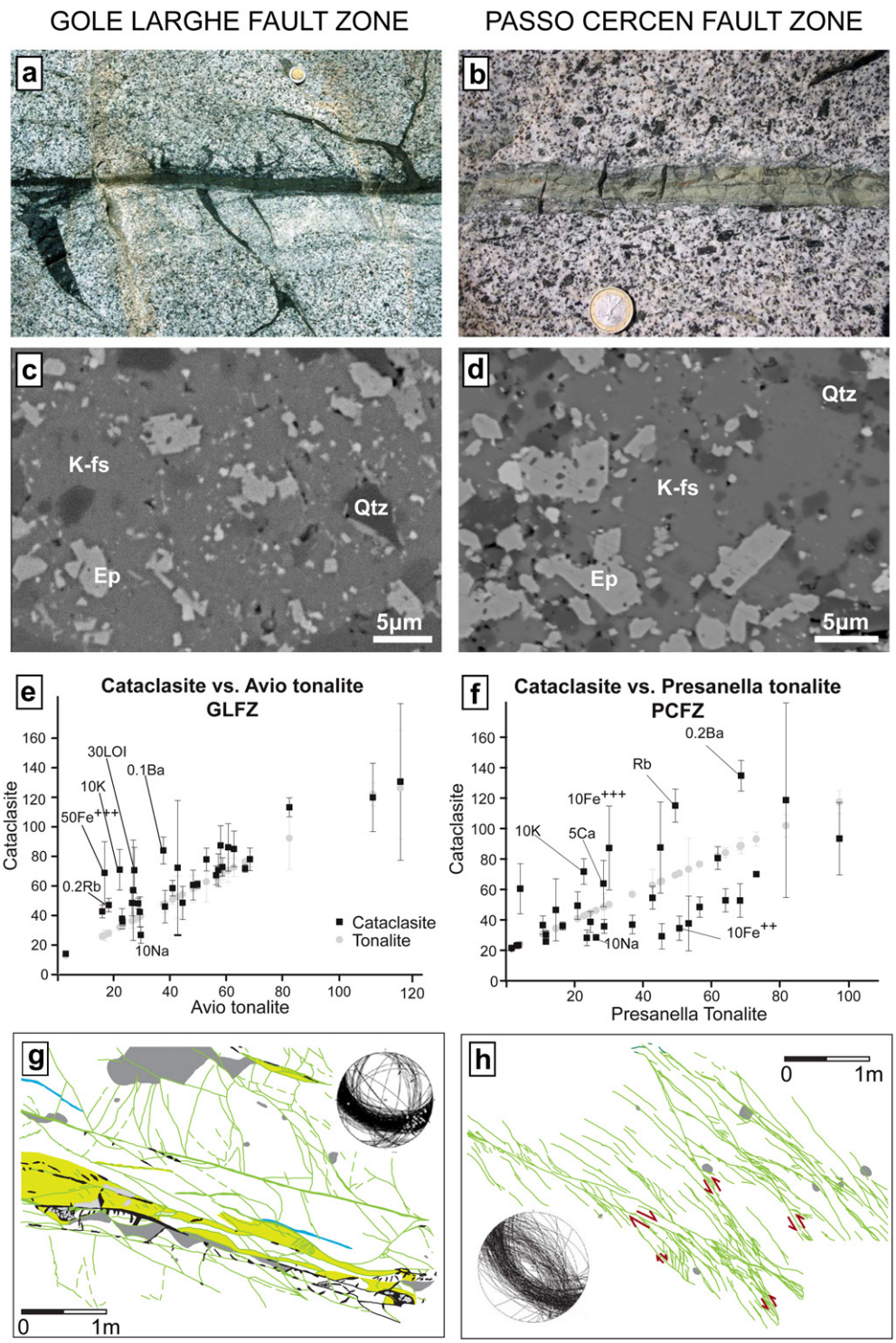

Fig. 9. Comparison of the main features of the GLFZ (left column) and PCFZ (right column). (a) and (b) Fault rock assemblage in the field: (a) a thin cataclasite is associated with a thick pseudotachylyte (GLFZ). (b) Thick cataclasite (PCFZ), in most cases pseudotachylytes are absent. (c) and (d) Cataclasite matrix under the SEM: mineral assemblages in the GLFZ (c) and PCFZ (d) are identical, with evidence for static growth of epidote (BSE-SEM images). (e) and (f) Elemental compositions from X-ray fluorescence analyses. The isocon diagrams (e.g. Grant, 2005) compare the elemental compositions of cataclasites (black dots) with that of the host tonalite (gray dots), normalized to the elemental composition of the host tonalite (Avio tonalite for the GLFZ, Presanella tonalite for the PCFZ); the shift of the cataclasite composition with respect to the host rock composition (host rock data form a straight line in the diagram) is proportional to the relative enrichment or loss of chemical components during hydrothermal alteration (and cementation) of cataclasites. Compared to the GLFZ, in the PCFZ the elemental composition of the cataclasites is more scattered with respect to the host tonalite. This geochemical evidence suggests a more intense chemical exchange with percolating fluids (XRF data of the GLFZ are from Di Toro and Pennacchioni, 2005). (g) and (h) Details of surface maps of the GLFZ (g) and the PCFZ (h), and cumulative stereoplots of all the fault data collected in the two fault zones; the legend is the same as in Fig. 5. Structural data for the GLFZ are from Di Toro and Pennacchioni (2005).

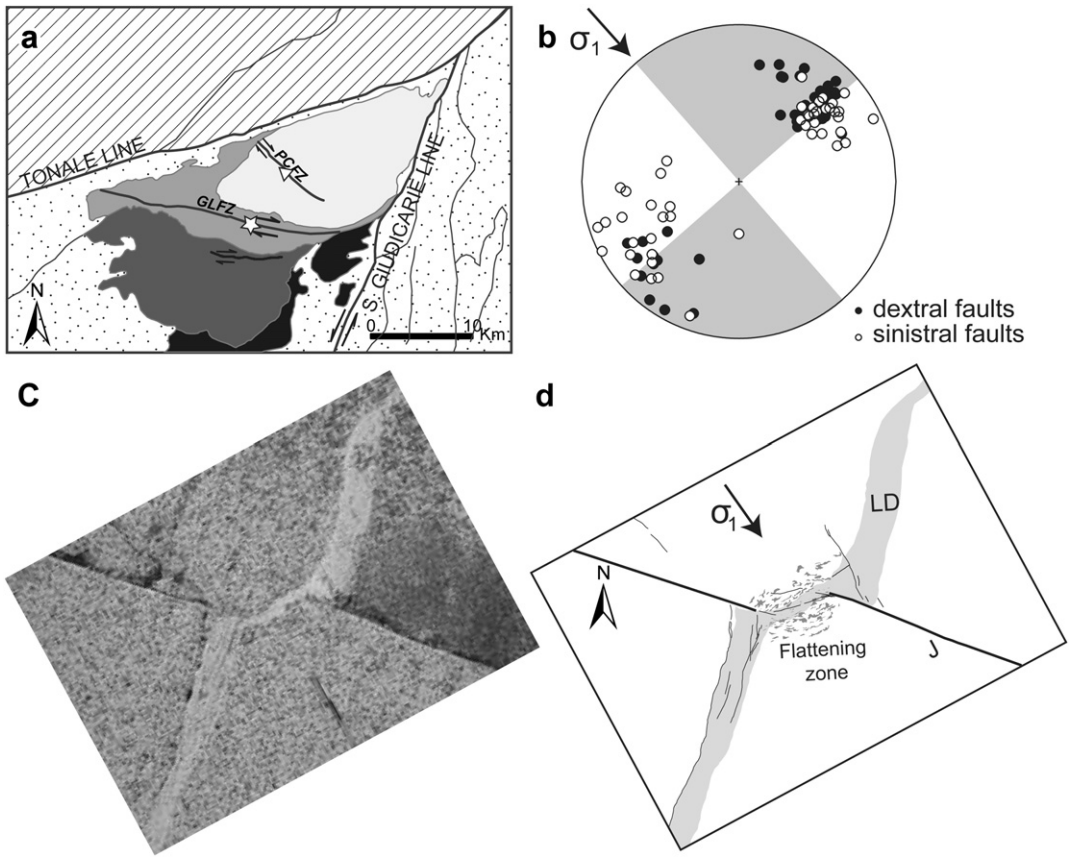

Fig. 10. Orientation of the regional maximum principal horizontal stress. (a) Geological sketch of the northern Adamello; the star indicates the Lobbia outcrop, where the field picture in Fig. 10c was taken, the triangle indicates the Passo Cercen area, where the structural data from the PCFZ were collected. (b) The orientation of the regional σ_1 as inferred from the switch in the shear sense of faults within the PCFZ. (c) Field photograph of a flattening zone developed at the intersection of two nearly orthogonal shear zones during amphibolite facies (T about 550 °C) deformation of the Avio tonalite (Lobbia outcrop), and (d) the same structure redrawn. The shear zones are localized along a joint (J) and a leucocratic dyke (LD). The orientation of σ_1 is similar to that inferred for the PCFZ.

Following McKenzie and Brune (1972), the heat flux generated per unit area of the fault is:

$$q \approx \mu\left(\sigma_n - p_p\right)V = \mu\sigma'_n V \tag{3}$$

where σ'_n is the effective normal stress acting on the fault plane and V is slip rate. The frictional heating depends on the friction coefficient, the velocity of sliding and the effective normal stress on the fault plane. The friction coefficient for granitoid rocks and the minerals cementing cataclasites (epidote + K-feldspar) is Byerlee-type, i.e. $0.6 < \mu < 0.85$, and minerals with significantly lower friction coefficient (e.g. talc, Byerlee, 1978) are absent in the studied faults. Slip rates were seismic in both fault zones, since the presence of pseudotachylyte is documented in both GLFZ and PCFZ.

The strength of the brittle crust depends on the ratio between the normal stress and shear stress acting on the fault plane and is described by the empirical Coulomb failure criterion (Sibson, 1990):

$$\tau = C + \mu_i\sigma'_n = C + \mu_i\left(\sigma_n - p_p\right) \tag{4}$$

where C is the cohesive strength, μ_i is the coefficient of internal friction, and τ is the resolved shear stress. For pre-existing cohesion-less faults, the fault strength is (Jaeger et al., 2007):

$$\tau = \mu\sigma'_n = \mu\left(\sigma_n - p_p\right) \tag{5}$$

(Amonton's law combined with Terzaghi's law), where μ is the friction coefficient. The reactivation of a cohesion-less fault whose pole lies in the σ_1/σ_3 plane is controlled by the ratio of effective principal stresses, which depends upon the angle θ_r within the fault plane and the direction of σ_1 (reactivation angle, Sibson, 1985):

$$R = \frac{\sigma'_1}{\sigma'_3} = \frac{\sigma_1 - p_p}{\sigma_3 - p_p} = \frac{1 + \mu\cot\theta_r}{1 - \mu\tan\theta_r} \tag{6}$$

This function has a positive minimum at

$$\theta_r{}^* = 0.5\tan^{-1}(1/\mu) = 26.5^\circ \tag{7}$$

defining the most favourable orientation for fault reactivation. If the angle θ_r departs more than 15° from $\theta_r{}^*$, the stress ratio to initiate sliding increases $b \sim 50\%$ and faults may be considered to be *unfavourably* oriented for reactivation (Sibson, 1990). Reactivation in these conditions is possible for low differential stresses and under elevated fluid pressure, with σ'_3 approaching 0; otherwise, the differential stress required for reactivation exceeds that needed to form a new fault (Sibson, 1985).

The GLFZ and the PCFZ are oriented at different angles with the inferred direction of σ_1 (Fig. 11a), the GLFZ being favorably oriented for reshear ($\theta_r \approx \theta_r{}^*$) and the PCFZ being oriented at $\theta_r << \theta_r{}^*$. The variations in effective normal stresses on the GLFZ and PCFZ have been estimated under the following assumptions and approximations:

(1) The coefficient of internal friction μ_i generally lies between 0.5 and 1.0 for rocks (Sibson, 1985), the coefficient of sliding friction is $0.6 < \mu < 0.85$ for most rocks (Byerlee, 1978); for

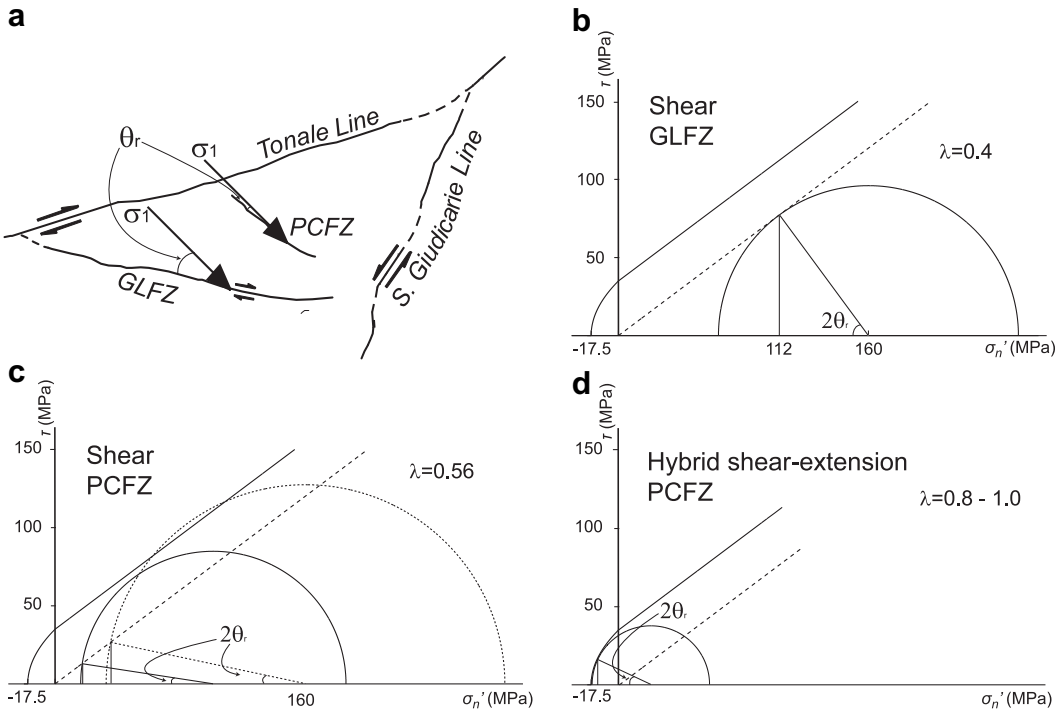

Fig. 11. Mechanics of the GLFZ and PCFZ. (a) The reactivation angle θ_r for the GLFZ and PCFZ. (b) Mohr analysis for the GLFZ. The failure envelopes for intact tonalite (solid line) and for reactivation of a cohesion-less fault (dashed line) have been drawn based on the parameters and boundary conditions discussed in the text. The conditions for failure are reached when the Mohr circle representing the state of stress of the fault zone strikes the failure envelope; the reactivation angle θ_r is half of the angle between the radius connecting the centre of the Mohr circle and the point of contact (labelled $2\theta_r$). For sliding along a fault oriented like the GLFZ, with a reactivation angle $\theta_r \approx 30^\circ$ and assuming hydrostatic pore pressure ($\lambda = 0.4$), the estimated effective stress normal to the fault plane is 112 MPa. (c) Plot of the state of stress for the PCFZ in Mohr space. Since the depth of faulting and thus σ_2 are the same as in the GLFZ, the Mohr circle can touch the failure envelope at an angle θ_r for $\lambda = 0.4$ and high differential stress (dotted circle) or for pore pressures higher than hydrostatic and lower differential stress (solid circle). For $\lambda = 0.56$ the estimated effective stress normal to the fault is on the order of 10–20 MPa. (d) The conditions for the formation of hybrid shear extension fractures in the PCFZ. The effective normal stress of the fault is tensile.

convenience, the failure of intact rock and the sliding failure envelopes have been drawn parallel with $\mu_i = \mu = 0.75$.

(ii) A cohesive strength $C = 35$ MPa has been chosen as representative for granitoid rocks (Amitrano and Schmittbuhl, 2002).

(iii) The faults are assumed to be vertical with pure strike–slip kinematics; averaged fault orientation is assumed to be N105° for the GLFZ and N130° ± 15° for the PCFZ.

(iv) The stress field is Andersonian (Di Toro et al., 2005), so that in a strike–slip regime, the effective vertical stress (σ'_v) corresponds to the intermediate principal stress (σ'_2), $\sigma'_v = \rho g z - p_p = \sigma'_2$ (Sibson, 1974), where ρ is the rock density, g is the acceleration due to gravity and z is the depth.

(v) The σ_1 and σ_3 axes are assumed to be horizontal and σ_1 strikes N135°, as inferred from the field evidence in the GLFZ and PCFZ.

(vi) The value of the intermediate principal stress is assumed to be $\sigma_2 = (\sigma_1 - \sigma_3)/2$, following Sibson (1974).

In the GLFZ, despite the extensive fluid–rock interaction in the cataclasites, there is no evidence for pervasive macroscopic veining. This field observation suggests that pore pressure was hydrostatic or lower (Di Toro et al., 2005). Assuming a depth $z = 10$ km and an average rock density of 2.65 g cm^{-3}, the effective vertical stress (and the effective intermediate normal stress) is $\sigma'_2 = \sigma'_v = \rho g z - p_p = \rho g z - \rho_w g z \approx 160$ MPa for a hydrostatic pore-fluid factor $\lambda = p_p/\rho g z = 0.4$ (Fig. 11a). The GLFZ makes an angle $\theta_r = 30^\circ \approx \theta_r{}^*$ with the inferred direction of σ_1. For reactivation of pre-existing joints, the effective normal stress acting on the fault plane is $\sigma' = 112$ MPa (Di Toro et al., 2005) (Fig. 11b).

In the PCFZ, the presence of pervasive macroscopic veining in the tonalite suggests that fluid pressure was locally higher than hydrostatic. The fault surfaces and epidote-bearing veins are mostly oriented at low angles to the σ_1 direction, with $\theta_r = 5 \pm 15^\circ$. The depth of faulting and the vertical stress $\sigma_v = \sigma_2$ are assumed to be the same as the GLFZ, but to allow reactivation of faults with this orientation or vein opening, it is necessary to assume either higher differential stresses or higher fluid pressures (Fig. 11c). The σ'_n on the PCFZ fault planes was thus significantly lower than in the GLFZ, since:

(i) For shear reactivation of joints, it is necessary to assume high differential stresses, or higher fluid pressure (Fig. 11c); in both cases, however, the σ'_n on fault planes is on the order of 10–20 MPa, significantly lower than in the GLFZ.

(ii) Tensional veins form in planes perpendicular to the least compressive stress σ_3, for $(\sigma_3 - p_p) = -T$ and $(\sigma_1 - \sigma_3) < 4T$, where $T = 0.5$ °C is the tensile strength of the rock (Price and Cosgrove, 1990). However, the veins in the PCFZ, striking at low angles to the σ_1 direction, are better described as hybrid extension and shear fractures, where $0.8 < (\sigma_3 - p_p) < T$ and $4T < (\sigma_1 - \sigma_3) < 5.5T$ (Price and Cosgrove, 1990). In both extension or hybrid fracture, the effective stresses on the fault planes is tensile, implying pore pressures approaching lithostatic values ($\lambda \approx 1.0$) (Fig. 11d).

This analysis suggest that effective normal stresses acting on the fault planes of the PCFZ were significantly lower than those inferred for the GLFZ, and that episodes of pore pressure approaching lithostatic values are likely in the PCFZ based on the observed field occurrence of extensive veining parallel to faults. It is therefore proposed that the production of frictional melting in the PCFZ was in most cases inhibited by: (i) low effective normal stresses acting on

fault planes, allowing only limited frictional heating; (ii) high fluid pressures, which, besides lowering the effective normal stresses for mechanical reasons, could also trigger weakening mechanisms such as thermal pressurization of fluids during earthquakes (Sibson, 1973; Lachenbruch, 1980; Bizzarri and Cocco, 2006; Rice, 2006); (iii) the presence of fluids in the slipping zone that adsorb a relevant amount of heat during frictional heating and buffer the increase in temperature.

Summarizing, field, geochemical and microstructural evidence suggests fluid–rock interaction during brittle deformation both in the PCFZ and in the GLFZ. However, alteration and veining are more intense in the PCFZ compared to the GLFZ (see Fig. 9e and f, Table 1). This suggests that in the PCFZ faulting occurred in a more fluid-rich environment, which possibly experienced build ups of fluid pressures higher than hydrostatic. The more intense fluid circulation in the PCFZ with respect to the nearby GLFZ could be a consequence of the different orientations of the pre-existing joints which localized the subsequent brittle deformation (Fig. 1b). In the Adamello batholith, the network of joints was the preferential pathway for fluid circulation, as suggested by the intense fluid–rock alteration found along joints and faults (e.g. Fig. 2), while the host tonalite was almost unaltered. The joints in the Presanella area (PCFZ) were oriented at low angles with respect to the inferred regional σ_1, and could have acted as dilational fractures, allowing greater amounts of fluid infiltration during faulting. Fluids could have been subsequently trapped and overpressurized by the precipitation of subgreenschist facies minerals (epidote, chlorite) in the fault zones. In contrast, the joints in the Avio area (GLFZ) were oriented at higher angles with respect to the regional σ_1, in a more compressive setting which might have impeded abundant fluid infiltration (Fig. 1b).

6. Conclusions

Two closely located fault zones (GLFZ and PCFZ) cutting the northern Adamello massif that were active at the same time and in the same regional stress field have been compared to highlight the factors affecting the formation of pseudotachylyte during seismic sliding. The most relevant difference between the two fault zones is their orientation, which is inferred to determine the different mechanics and resulting fault rock assemblages. The GLFZ strikes at ca. 30° to the inferred regional σ_1, being active under high normal stresses (ca. 100 MPa) and low (i.e. hydrostatic) fluid pressures: the fault rock assemblage includes abundant pseudotachylytes. The PCFZ strikes almost parallel to the σ_1 direction, allowing lower (10–20 MPa) normal stresses and higher fluid infiltration (up to fluid pressure higher than hydrostatic). Frictional heating is proportional to the normal stress resolved on the fault plane. Under low normal stresses, such as those developed along the PCFZ, melting could be reached only locally. The fault rock assemblage is associated with abundant epidote-bearing veins and cataclasites, but few pseudotachylytes. Other seismically activated processes, such as thermal pressurization of pore fluids may have further inhibited the frictional heating along the PCFZ.

Acknowledgements

Many thanks to Leonardo Tauro and Antonio Novello (thin sections preparation), Federico Zorzi (XRD), Daria Pasqual (XRF), Luca Peruzzo (SEM), Andrea Cavallo and Piergiorgio Scarlato (FE-SEM at INGV in Rome) and Stefano Castelli (image acquisition). The people of the Museo Tridentino di Scienze Naturali, especially Marco Avanzini, are thanked for the constant support and the stimulating discussions. The Servizio Meteorologico della Provincia di Trento kindly provided high resolution aerial photographs of the northern Adamello. The constructive reviews and comments of Robert Holdsworth and Zoe Shipton improved substantially the manuscript and addressed very interesting topics. Mirko and Erika Dezulian of the Francesco Denza mountain hut (Vermiglio, Trento) are also greatly acknowledged. This study was founded by the Fondazione CARITRO, by the CA.RI.PA.RO Project (progetti di Eccellenza 2006) and by the European Research Council Starting Grant project USEMS (Nr. 205175).

References

Abercrombie, R., McGarr, A., Kanamori, H., Di Toro, G. (Eds.), 2006. Earthquakes: Radiated Energy and the Physics of Faulting. Geophysical Monograph Series, 170. AGU.

Amitrano, D., Schmittbuhl, J., 2002. Fracture roughness and gouge distribution of a granite shear band. Journal of Geophysical Research 107, B12. doi:10.1029/2002JB001761.

Andrews, D.J., 2002. A fault constitutive relation accounting for thermal pressurization of pore fluid. Journal of Geophysical Research 107 (B12), 2363. doi:10.1029/2002JB001942.

Bianchi, A., Callegari, E., Jobstraibizer, P.G., 1970. I tipi petrografici fondamentali del plutone dell'Adamello (tonaliti, quarzodioriti, granodioriti e loro varietà leucocrate). Memorie dell'Istituto di Geologia e Mineralogia dell'Università di Padova 27, 1–148.

Bizzarri, A., Cocco, M., 2006. A thermal pressurization model for the spontaneous dynamic rupture propagation on a three-dimensional fault: 1. Methodological approach. Journal of Geophysical Research 111, B05303. doi:10.1029/2005JB003862.

Brack, P., 1983. Multiple intrusions – examples from the Adamello batholith (Italy) and their significance on the mechanisms of intrusion. Memorie della Società Geologica Italiana 26, 145–157.

Byerlee, J.D., 1978. Friction of rocks. Pure and Applied Geophysics 116, 615–626.

Castellarin, A., Cantelli, L., 2000. Neo-Alpine evolution of the Southern Eastern Alps. Journal of Geodynamics 30, 251–274.

Castellarin, A., Vai, G.B., Cantelli, L., 2006. The alpine evolution of the Southern Alps around the Giudicarie faults: a Late Cretaceous to Early Eocene transfer zone. Tectonophysics 414, 203–223.

Cowan, D.S., 1999. Do faults preserve a record of seismic slip? A field geologist's opinion. Journal of Structural Geology 21, 995–1001.

De Capitani, L., Delitala, M.C., Liborio, G., Mottana, A., Rodeghiero, F., Thöni, M., 1994. The granitoid rocks of Val Navazze, Val Torgola and Val di Rango (Val Trompia, Lombardy, Italy). Memorie di Scienze Geologiche 46, 329–343.

Del Moro, A., Pardini, G., Quercioli, C., Villa, I.M., Callegari, E., 1983. Rb/Sr and K/Ar chronology of Adamello granitoids, southern Alps. Memorie della Società Geologica Italiana 26, 285–299.

Di Toro, G., Pennacchioni, G., 2004. Superheated friction-induced melts in zoned pseudotachylytes within the Adamello tonalites (Italian Southern Alps). Journal of Structural Geology 26, 1783–1801.

Di Toro, G., Pennacchioni, G., 2005. Fault plane processes and mesoscopic structure of a strong-type seismogenic fault in tonalites (Adamello batholith, Southern Alps). Tectonophysics 402, 55–80.

Di Toro, G., Pennacchioni, G., Teza, G., 2005. Can pseudotachylytes be used to infer earthquake source parameters? An example of limitations in the study of exhumed faults. Tectonophysics 402, 3–20.

Di Toro, G., Pennacchioni, G., Nielsen, S., 2009. Pseudotachylytes and earthquake source mechanics. In: Fukuyama, Eiichi (Ed.), Fault-Zone Properties and Earthquake Rupture Dynamics. International Geophysics Series. Elsevier.

Grant, J.A., 2005. Isocon analysis: a brief review of the method and applications. Physics and Chemistry of the Earth 30, 997–1004.

Hansmann, W., Oberli, F., 1991. Zircon inheritance in an igneous rock suite from the southern Adamello batholith (Italian Alps). Contributions to Mineralogy and Petrology 107, 501–518.

Imber, J., Holdsworth, R.E., Butler, C.H., Strachan, R.A., 2001. A reappraisal of the Sibson–Scholz fault zone model: the nature of the frictional to viscous (''brittle–ductile'') transition along a long-lived, crustal-scale fault, Outer Hebrides, Scotland. Tectonics 20 (5), 601–624.

Jefferies, S.P., Holdsworth, R.E., Wibberley, C.A.I., Shimamoto, T., Spiers, C.J., Niemeijer, A.R., Lloyd, G.E., 2006. The nature and importance of phyllonite development in crustal-scale fault cores: an example from the Median Tectonic Line, Japan. Journal of Structural Geology 28, 220–235.

Kirkpatrick, J.D., Shipton, Z.K., Persano, C., 2009. Pseudotachylytes: rarely generated, rarely preserved or rarely reported? Bulletin of the Seismological Society of America 99, 382–388.

Kostrov, B., Das, S., 1988. Principles of Earthquake Source Mechanics. Cambridge University Press, London.

Jaeger, J.C., Cook, N.G.W., Zimmerman, R.W., 2007. Fundamentals of Rock Mechanics. Blackwell Publishing.

John, B.E., Blundy, J.D., 1993. Emplacement-relate deformation of granitoid magmas, southern Adamello Massif, Italy. Geological Society of America Bulletin 105, 1517–1541.

Lachenbruch, A.H., 1980. Frictional heating, fluid pressure and the resistance to fault motion. Journal of Geophysical Research 85, 6097–6112.

Lockner, D.A., Okubo, P.G., 1983. Measurements of frictional heating in granite. Journal of Geophysical Research 88, 4313–4320.

Magloughlin, J.F., Spray, J.G., 1992. Frictional melting processes and products in geological materials: introduction and discussion. Tectonophysics 204, 197–206.
Martin, S., Zattin, M., Del Moro, A., Macera, P., 1996. Chronologic constraints for the evolution of the Giudicarie belt (Eastern Alps, NE Italy). Annales Tectonicae 10, 60–79.
Mayer, A., Cortiana, G., Dal Piaz, G.V., Deloule, E., De Pieri, R., Jobstraibizer, P., 2003. U–Pb single zircon ages of the Adamello batholith, Southern Alps. Memorie di Scienze Geologiche 55, 151–167.
McKenzie, D., Brune, J.N., 1972. Melting on fault planes during large earthquakes. Geophysical Journal of the Royal Astronomical Society 29, 65–78.
Passchier, C.W., Trouw, R.A.J., 2005. Microtectonics, second ed. Springer, Berlin.
Pennacchioni, G., 2005. Control of the geometry of precursor brittle structures on the type of ductile shear zone in the Adamello tonalites, Southern Alps (Italy). Journal of Structural Geology 27, 627–644.
Pennacchioni, G., Di Toro, G., Brack, P., Menegon, L., Villa, I.M., 2006. Brittle–ductile–brittle deformation during cooling of tonalite (Adamello, Southern Italian Alps). Tectonophysics 427, 171–197.
Pennacchioni, G., Mancktelow, N., 2007. Nucleation and initial growth of a shear zone network within compositionally and structurally heterogeneous granitoids under amphibolite facies conditions. Journal of Structural Geology 29, 1757–1780.
Pittarello, L., Di Toro, G., Bizzarri, A., Pennacchioni, G., Hadizadeh, J., Cocco, M., 2008. Energy partitioning during seismic slip in pseudotachylyte-bearing faults (Gole Larghe Fault, Adamello, Italy). Earth and Planetary Science Letters 269, 131–139. doi:10.1016/j.epsl.2008.01.052.
Price, N.J., Cosgrove, J.W., 1990. Analyses of Geological Structures. Cambridge University Press.
Rice, J.R., 2006. Heating and weakening of faults during earthquake slip. Journal of Geophysical Research 111, B05311. doi:10.1029/2005JB004006.
Riklin, K., 1985. Contact metamorphism of Permian "red sandstones" in the Adamello area. Memorie della Società Geologica Italiana 26, 159–169 (1983).
Salomon, W., 1897. Über Alter, Lagerungsform und Entstehungsart der periadriatischen granitisch-körnigen Massen. Tschermaks mineralogische und petrographische Mitteilungen 17 (H 2/3), 109–284.
Scholz, C.H., 1988. The brittle–plastic transition and the depth of seismic faulting. Geologische Rundschau 77, 319–328.
Scholz, C.H., 2002. The Mechanics of Earthquakes and Faulting, second ed. Cambridge University Press.
Schmid, S.M., Aebli, H.R., Heller, F., Zingg, A., 1989. The role of the Periadriatic Line in the tectonic evolution of the Alps. In: Coward, M.P., Dietrich, D., Park, R.G. (Eds.), Alpine Tectonics. Geological Society Special Publication 45, pp. 153–171.
Sibson, R.H., 1973. Interactions between temperature and pore fluid pressure during earthquake faulting – a mechanism for partial or total stress relief. Nature 243, 66–68.
Sibson, R.H., 1974. Frictional constraints on thrust, wrench and normal faults. Nature 249, 542–544.
Sibson, R.H., 1975. Generation of pseudotachylyte from ancient seismic faulting. Geophysical Journal of the Royal Astronomical Society 43, 775–794.
Sibson, R.H., 1977. Fault rocks and fault mechanisms. Journal of the Geological Society 133 (3), 191–213.
Sibson, R.H., 1985. A note on fault reactivation. Journal of Structural Geology 7, 751–754.
Sibson, R.H., 1986. Brecciation processes in fault zones: inferences from earthquake rupturing. Pure and Applied Geophysics 124, 159–175.
Sibson, R.H., 1990. Rupture nucleation on unfavorably oriented faults. Bulletin of the Seismological Society of America 80, 1580–1604.
Sibson, R.H., Toy, V.G., 2006. The habitat of fault generated pseudotachylyte: presence vs. absence of frictional melt. In: Abercrombie, R., McGerr, A., Kanamori, H., Di Toro, G. (Eds.), Earthquakes: Radiated Energy and the Physics of Faulting. Geophysical Monograph Series, 170. AGU, pp. 153–166.
Spray, J.G., 1995. Pseudotachylyte controversy: fact or friction? Geology 23, 1119–1122.
Stipp, M., Stünitz, H., Heilbronner, R., Schmid, S.M., 2002. The eastern Tonale fault zone: a 'natural laboratory' for crystal plastic deformation of quartz over a temperature range from 250 °C to 700 °C. Journal of Structural Geology 24, 1861–1884.
Stipp, M., Fügenschuh, B., Gromet, L.P., Stünitz, H., Schmid, S.M., 2004. Contemporaneous plutonism and strike slip faulting: a case study from the Tonale fault zone north of the Adamello pluton (Italian Alps). Tectonics 23, TC3004. doi:10.1029/2003TC001515.
Trener, G.B., 1906. Geologische Aufnahme in nördlichen Abhang der Presanellagruppe. Jahrbuch der Kaisaerlich-königlichen geologische Reichsanstalt 56, 405–496.
Villa, I.M., Hermann, J., Müntener, O., Trommsdorff, V., 2000. 39Ar–40Ar dating of multiply zoned amphibole generations (Malenco, Italian Alps). Contributions to Mineralogy and Petrology 140, 363–381.
Viola, G., 2000. Kinematics and timing of the Periadriatic fault system in the Giudicarie region (central-eastern Alps). PhD thesis, ETH Zürich, Nr. 13590.
Viola, G., Mancktelow, N.S., Seward, D., 2001. Late Oligocene–Neogene evolution of Europe–Adria collision: new structural and geochronological evidence from the Giudicarie fault system (Italian Eastern Alps). Tectonics 20, 999–1020.
Werling, E., 1992. Tonale-, Pejo- und Judicarien-Linien: Kinematik, Mikrostrukturen und Metamorphose von Tektoniten aus räumlich interferienden aberverschiedenaltrigen Verwerfungszonen. PhD thesis, ETH, Zürich.
Woodcock, N.H., Mort, K., 2008. Classification of fault breccias and related fault rocks. Geological Magazine 145, 435–440.